ChemPubSoc Europe

DOI: 10.1002/cphc.201402137

Evaluation of Perovskites as Electrocatalysts for the Oxygen Evolution Reaction

Rosalba A. Rincón,[a] Edgar Ventosa,[a] Frank Tietz,[b] Justus Masa,[a] Sabine Seisel,[a] Volodymyr Kuznetsov,[a] and Wolfgang Schuhmann*[a]

The oxygen evolution reaction (OER) is an enabling process for technologies in the area of energy conversion and storage, but its slow kinetics limits its efficiency. We performed an electrochemical evaluation of 14 different perovskites of variable composition and stoichiometry as OER electrocatalysts in alkaline media. We particularly focused on improved methods for a reliable comparison of catalyst activity. From initial electrochemical results we selected the most active samples for further optimization of electrode preparation and testing. An inverted cell configuration facilitated gas bubble detachment and thus minimized blockage of the active surface area. We describe parameters, such as the presence of specific cations, stoichiometry, and conductivity, that are important for obtaining electroactive perovskites for OER. Conductive additives enhanced the current and decreased the apparent overpotential of OER for one of the most active samples ($La_{0.58}Sr_{0.4}Fe_{0.8}Co_{0.2}O_3$).

1. Introduction

Energy conversion and storage are currently the critical barriers in the efficient utilization of renewable energy sources that produce intermittent power (i.e. solar and wind). In recent years, the increased interest in the direct conversion of solar and wind energy into storable fuels has raised research efforts with respect to the optimization of energy storage devices. In addition, portable electronic devices (e.g. cell phones, digital cameras, laptop computers, and tablets) have been developing at a fast pace, demanding higher energy and power densities of the in-built power sources. Thus, research in the area of batteries and fuel cells has largely grown in the past decade.

Oxygen reduction and oxygen evolution are essential electrochemical reactions in rechargeable metal–air batteries, fuel cells, water electrolyzers, chlor-alkali cells, and CO_2 reduction. The kinetics of both reactions represents a critical challenge for the practical realization of these technologies. Electrocatalysis to facilitate the oxygen reduction reaction (ORR) has been a major research topic and many advances have been empirically made in this area towards finding low cost highly active catalysts. Intense research was carried out on different catalyst materials in the 1950 s and 1960 s to understand the mechanisms of the oxygen evolution reaction (OER),[1] but the main focus was pointed towards the ORR, as reflected in the number of publications. However, the efforts in optimizing OER with improved and low-cost catalysts have regained interest recently.

The slow kinetics of the OER is an important topic in electrocatalysis, and consequently for metal–air batteries, water electrolyzers, and H_2/O_2 fuel cells, limiting their efficiencies due to power losses by more than 15%.[2] In the past, electrocatalysts for the OER have been restricted to noble metals (e.g. Pt, Ru, Ir, and Pd) and their alloys. Later studies have shown that improved OER was due to the presence of a thick oxide film on the surface of the noble metals.[3] Thus, the use of various mixed oxides represents an important focal point in the research for OER catalysts. This includes catalysts based on a mixture of IrO_2 and Pt;[4] mixtures of IrO_2 and TiO_2;[5] mixtures of IrO_2 and SnO_2;[6] IrO_2;[7] RuO_2,[8] and a mixture of both. However, the costs of precious metals are very high for large-scale applications, limiting their practical use. Therefore, research has been devoted to lowering the load of precious metals in electrocatalysts or replacing them completely.

Research efforts have been focused on low-cost transition-metal oxides as an alternative to precious-metal-based materials. Among these MnO_2,[9] $NiCO_2O_4$,[10] $La_{1-x}Sr_xMnO_3$,[11] $La_{1-x}Sr_xCoO_3$,[12] and $La_{1-x}Mn_xCoO_3$[13] were investigated. The use of perovskite-type oxides is well-known for high temperature solid oxide fuel cell (SOFC) applications,[14] but there have also been reports of their use for OER in alkaline media.[15] Their electrocatalytic activities towards OER have been studied to a certain extent since the first publications regarding OER appeared[16] and they have recaptured interest over the past few years.[17–19] The activity of several perovskite materials for OER and ORR has been ranked in so-called volcano plots using different theoretical descriptors.[20]

Due to their chemical structure (ABO_3) and non-stoichiometric composition, perovskites have semiconductive and even

[a] Dr. R. A. Rincón, Dr. E. Ventosa, Dr. J. Masa, Dr. S. Seisel, Dr. V. Kuznetsov, Prof. Dr. W. Schuhmann
Analytische Chemie—Elektroanalytik & Sensorik
Ruhr Universität-Bochum
Universitätsstr. 150, 44780 Bochum (Germany)
E-mail: wolfgang.schuhmann@rub.de

[b] Dr. F. Tietz
Forschungszentrum Jülich GmbH, IEK-1
52425 Jülich (Germany)

metallic conductivity.[2] Moreover, their physico-chemical and catalytic properties can be modified because it is possible to substitute ions of the same or different oxidation states in the A and B sites.[21] Thus, perovskites are interesting materials for fundamental electrocatalysis studies with the aim of establishing correlations between physico-chemical and electrocatalytic properties. Numerous theoretical approaches were developed in order to find activity descriptors to predict the electrocatalytic tendencies of these types of materials. Matsumoto et al.[11,12] developed the theory of σ* band formation, which explains that for high OER catalytic activities the perovskites form a broad σ* band and that the transition metal cation exists in a higher oxidation state. Trasatti[22] proposed that the plot of overpotentials as a function of the enthalpy change for the lower-to-higher oxide transition in the catalyst follows, to some extent, a volcano-shaped curve. Bockris and Otagawa[16] found that the catalytic activity of perovskites increases with higher occupancy of the antibonding orbitals of M^z-OH. More recently, Rossmeisl et al.[23] proposed the difference in binding energies between the reaction intermediates HOO* and HO* as a universal descriptor for the activity of a wide range of oxides (rutile, perovskite, spinel, rock salt, and bixbyite) towards OER. All of these theoretical models have paved the way and provided numerous possibilities to investigate potential perovskite-type electrocatalysts for OER, leading to an increased number of recent publications involving different perovskites for OER.[15]

In this work we evaluated the electrocatalytic activity of different perovskite-type materials towards OER; some of which had been previously tested as SOFC cathode materials[14,24,25] and demonstrated to be active at high temperatures. The general chemical formula of the studied perovskites is $A_{1-x}A'_xB_{1-y}B'_yO_3$ and $A_{1-x}A'_xBO_3$, in which A and A′ is a rare-earth metal or an alkaline-earth metal, and B and B′ are transition metals. Our goal was to identify the critical structural and compositional parameters that influence the OER activity of these materials, and to find improved conditions for reliable electrochemical characterization of the catalysts. We also investigated possibilities for enhancing the conductivity of the materials and thereby their catalytic properties.

2. Results and Discussion

2.1. Physicochemical Characterization

The electrocatalytic activity towards the OER of fourteen different perovskites of variable composition and stoichiometry was investigated with the aim of identifying key parameters that influence their activity. Table 1 shows a list of all the perovskite-type oxides used in this work with their chemical formulas and the Brunauer—Emmett–Teller (BET) surface areas.

X-ray diffraction (XRD) and particle size distribution are henceforth only shown for the most electrochemically active samples. XRD patterns of the synthesized compositions showed that the powders were pure perovskites after the heat treatment at $T = 1100\,^{\circ}C$ (Figure 1).

Table 1. List of perovskite samples studied with their chemical formulas and BET surface areas (static, N_2).

Abbreviation	Formula	BET [$m^2 g^{-1}$]
LSMC	$La_{0.75}Sr_{0.2}Mn_{0.9}Co_{0.1}O_3$	1.6
PSM	$Pr_{0.65}Sr_{0.3}MnO_3$	1.8
LSMCr	$La_{0.7}Sr_{0.25}Mn_{0.5}Cr_{0.5}O_3$	1.0
L58SF	$La_{0.58}Sr_{0.4}FeO_3$	1.6
L60SF	$La_{0.6}Sr_{0.4}FeO_3$	1.8
L78SF	$La_{0.78}Sr_{0.2}FeO_3$	1.5
L58SCF	$La_{0.58}Sr_{0.4}Co_{0.2}Fe_{0.8}O_3$	0.6
L74SCF	$La_{0.74}Sr_{0.2}Co_{0.2}Fe_{0.8}O_3$	0.7
L76SCF	$La_{0.76}Sr_{0.2}Co_{0.2}Fe_{0.8}O_3$	0.8
L78SCF	$La_{0.78}Sr_{0.2}Co_{0.2}Fe_{0.8}O_3$	0.9
L58SCCF	$La_{0.58}Sr_{0.4}Co_{0.2}Cu_{0.1}Fe_{0.7}O_3$	—[a]
LCaMC	$La_{0.83}Ca_{0.15}Mn_{0.6}Co_{0.4}O_3$	0.7
LSM	$La_{0.65}Sr_{0.3}MnO_3$	1.9
LMCCu	$La_{0.97}Mn_{0.4}Co_{0.3}Cu_{0.3}O_3$	0.1

[a] Surface area was too low to measure.

Apart from $La_{0.83}Ca_{0.15}Mn_{0.6}Co_{0.4}O_3$ (LCaMC), which crystallized with an orthorhombic structure, the diffraction patterns of all other perovskites could be indexed with the rhombohedral (hexagonal) structure (Table 2). The BET surface area values for all samples were low (below 2 $m^2 g^{-1}$, see Table 1); hence the error of the measurements was large. The particle size distribution of selected perovskites (Figure 2, Table 3) shows values between 1 and 10 μm, which explains the low BET surface areas and the narrow widths of the XRD reflections further confirm the large size of the perovskite particles.

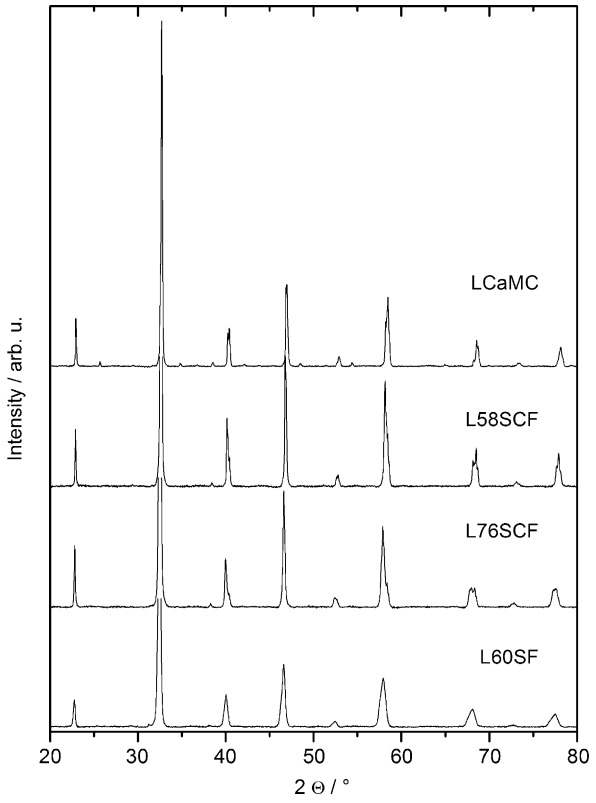

Figure 1. XRD patterns of selected perovskites.

Table 2. Lattice parameters of selected perovskites.

Compound	Space group	a [Å^{-1}]	b [Å^{-1}]	c [Å^{-1}]
LCaMC	*Pnma*	5.4576(1)	7.7249(1)	5.4915(1)
L76SCF	R-3c	5.5240(2)	-	13.4149(4)
L58SCF	R-3c	5.4977(1)	-	13.3808(2)
L60SF	R-3c	5.5199(3)	-	13.452(1)

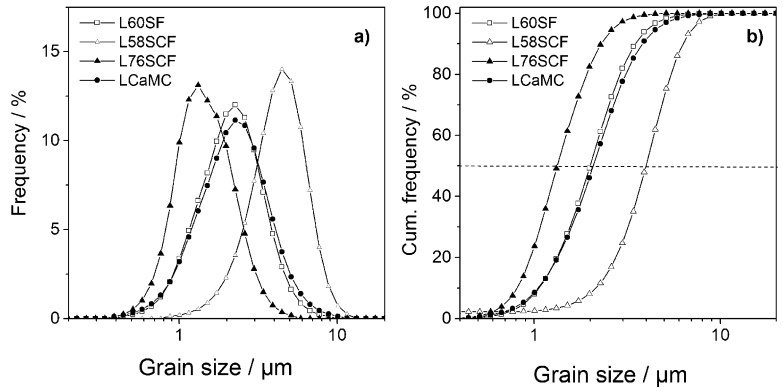

Figure 2. Particle-size distribution of four selected perovskites (a) and the corresponding cumulative frequency (b) as determined by laser diffraction analysis. The dashed line indicates the median particle size (D_{50}).

Table 3. Characteristic particle-size values for the four perovskites.

Compound	D_{10} [μm]	D_{50} [μm]	D_{90} [μm]
LCaMC	1.05	2.08	3.82
L76SCF	0.81	1.33	2.29
L58SCF	2.17	3.98	6.32
L60SF	1.06	2.00	3.50

2.2. Initial Electrochemical Characterization

To identify suitable electrocatalysts for the OER in alkaline media, fourteen perovskite samples were electrochemically tested by cyclic voltammetry (CV).

The potential was swept in the anodic direction to values close to 2.0 V versus the reversible hydrogen electrode (RHE). Figure 3 shows a summary of this initial characterization towards the OER, by comparing the total current obtained at the same potential (1.8 V vs. RHE) at which the OER was already observed for the active materials. Normalization of the catalytic current by geometric surface area or mass loading can be misleading, because the same mass loading of catalyst per surface area of the electrode ($\approx$200 μg cm^{-2}) was used for all samples on electrodes of equal size.

Estimation of the real surface area of a catalyst is a challenge when working with catalyst powders prepared as inks, because a lot of different factors come into play; namely particle size, surface roughness, and the catalyst area that is exposed or wet, as well as the electrochemically active surface area. Moreover, calculation of the electrochemically accessible surface area by estimating the capacitive current would be ideal, but is possible only if the specific capacitance of each material is known. In the case of perovskites we assume specific capacitance values and therefore the corresponding error would be quite large, as observed in the past by Bockris.[16] Under these conditions, normalizing the current by any surface area value would bring uncertainties and can misinform the reader; therefore, we only compare total currents.

Eight samples demonstrated catalytic activity towards the OER. In decreasing order of current output they were: L58SCF > L76SCF > LCaMC > L60SF > L74SCF > LSCCuF > LSMC > LMCCu. From the samples that had been previously tested as SOFC cathodes, L58SCF also presented the highest activity at high temperatures,[25] which could give us a hint when looking into potential OER electrocatalysts. PSM, L78SCF, LSMCr, L78SF, L58SF, and LSM showed no catalytic activity towards the OER. Samples were considered active if the OER currents were above 20 μA at 1.8 V (vs. RHE), because approximately 20 μA corresponds to the current observed for blank electrodes (glassy carbon with Nafion layer). The current shown by the blank electrodes may be a combination of the capacitive current and small contribution for the OER from glassy carbon (GC). In general, all samples with significant catalytic activity contained La as one of the cations on the A-site and seven out of eight contained Co as one of the cations on the B-site. The two catalysts with the highest catalytic activity (L58SCF and L76SCF) contained Sr and Fe as the second cation on the A- and B-site, respectively. Notably, sam-

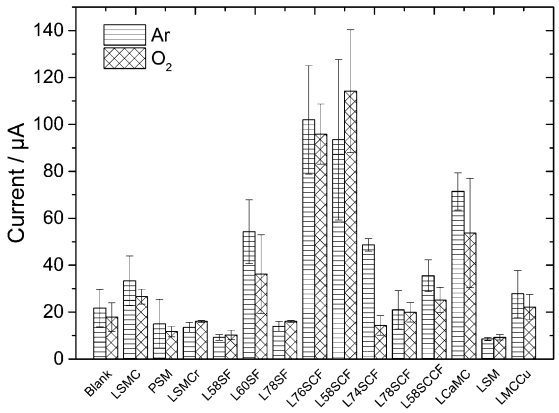

Figure 3. Electrochemical characterization of different perovskite-type oxides, showing current at 1.8 V (vs. RHE) in alkaline media (0.1 M NaOH). Data obtained from CV recorded at 5 mV s^{-1}.

ples with the same cations but slightly different compositions (e.g. L58SF, L60SF, and L78SF), showed completely different catalytic activities (L58SF and L78SF showed no activity towards OER). Hence, we concluded that in addition to the presence of specific cations, the stoichiometry of the perovskite also plays an important role in determining its catalytic activity, most likely due to changes in the state of charge of each sample. Slight changes in stoichiometry among L58SF, L60SF, and L78SF gave large changes in their catalytic activity. The same behavior was observed for the group of L58SCF, L74SCF, L76SCF, and L78SCF, in which minor variations in stoichiometry resulted in very different catalytic activities.

After identifying the catalysts that were active towards OER in alkaline media, additional experiments were carried out in order to further study their electrocatalytic properties.

2.3. Atomic Force Microscopy: Catalyst Loss Visualization

One of the main challenges of studying gas-evolving reactions is the generation of bubbles, which may partially block the active surface of the catalyst or electrode and may also lead to degradation by detachment of the catalyst itself. This observation was confirmed by atomic force microscopy (AFM) studies performed before and after subjecting a sample to consecutive CVs. Figure 4 shows the surface topography of a dried perovskite suspension on GC electrodes. A freshly prepared, modified electrode using L58SCF showed a multilayer structure with conglomerates of perovskite particles (see Figure 4a). In contrast, after 20 CVs the surface was covered mainly with small conglomerates and single particles (cf. Figure 4b). From similar images we estimated the range of single particle height distribution as 0.2–1.5 μm. Moreover, the thickness of the Nafion layer, 20 ± 4 nm, was determined by nanolithographical scratching and subsequent AFM imaging.

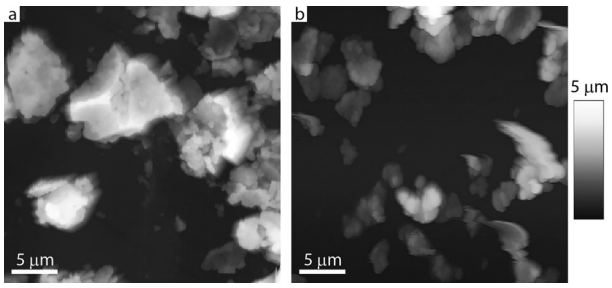

Figure 4. AFM images of a dried perovskite suspension (L58SCF) on a GC electrode before (a) and after (b) cyclic voltammetry in electrode facing downwards configuration. The particle density decreased after 20 CVs in a potential range between 0 and 2 V (vs. RHE) at 5 mV s^{-1}.

2.4. Optimization Experiments with Selected Perovskites

To avoid the high blockage of the electrode surface by evolved bubbles and catalyst detachment due to the pressure exerted by gas bubbles, we have implemented a "facing upwards" electrode configuration, which facilitates bubble departure. Although a large number of bubbles still accumulated on the surface of the electrode during electrochemical experiments, it was visibly lower than the blockage of the electrode surface during the experiments in which the electrode was facing downwards. This observation was validated when comparing the achieved current values, which were higher for the electrode facing upwards. Figure 5 shows the comparison of the current at 1.8 V (vs. RHE) for the four most active samples: L60SF, L58SCF, L76SCF, and LCaMC, between both cell configurations. The increase in current obtained is higher for L60SF, L76SCF, and L58SCF representing a 5-fold, 4-fold, and 2-fold increase, respectively, whereas for LCaMC the increase in current is not significant. However, we consider this strategy an overall improvement for the bubble detachment during oxygen evolution.

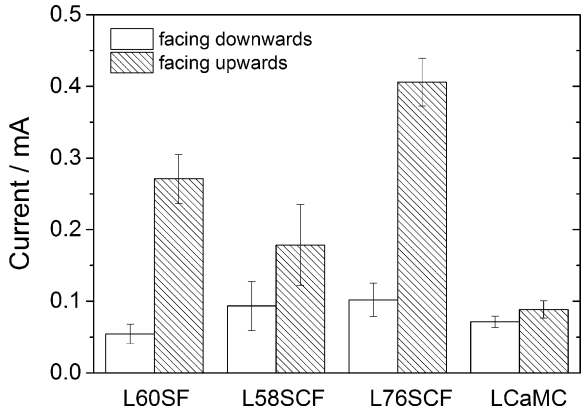

Figure 5. Comparison of the current obtained at 1.8 V (vs. RHE) in alkaline media for selected samples using different cell configurations (electrode facing downwards vs. electrode facing upwards). Data obtained from CVs recorded at 5 mV s^{-1}.

Figure 6a shows representative CVs for L60SF, L58SCF, L76SCF, and LCaMC after ohmic drop correction, and Figure 6b shows Tafel plots for the same samples. An apparent onset potential of approximately 1.58 V (vs. RHE) was observed for L60SF and L76SCF, and of approximately 1.63 V (vs. RHE) for L58SCF and LCaMC, which corresponded to an overpotential of 350 to 400 mV with respect to the thermodynamic OER potential. These values were 150 to 200 mV higher than the overpotential for OER when using commercial RuO_2 as the catalyst (observed experimentally, data not shown). These results were comparable to recent reports for other perovskite materials,[17] however with lower activity than the reported catalysts with overpotentials below 200 mV.[18]

To further improve the electrode preparation method, a conductive additive was added to increase the amount of active sites on the electrocatalysts in electronic contact with the electrode. Carbon blacks (CBs) were chosen due to their high conductivity and high specific surface area. Figure 7 shows a comparison of CVs obtained for two of the most active catalysts (L60SF and L58SCF), and the corresponding Tafel plots. A 1.7-fold and 2.3-fold increase was observed for L60SF and L58SCF, respectively, upon addition of CBs (current values compared at

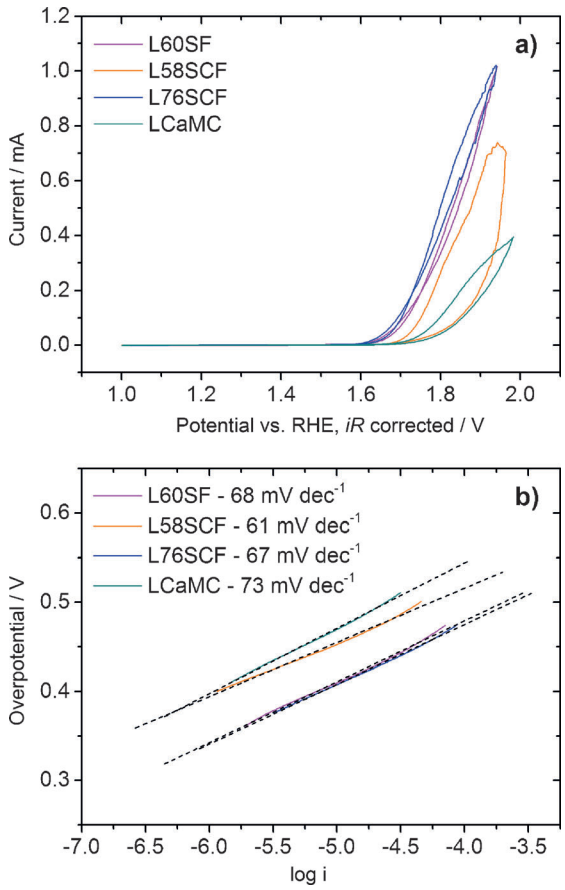

Figure 6. a) Representative CVs of L60SF, L58SCF, L76SCF, and LCaMC in 0.1 M KOH. Scan rate: 5 mV s^{-1}. b) Tafel plots obtained from linear sweep voltammetry (LSV) recorded at 1 mV s^{-1}.

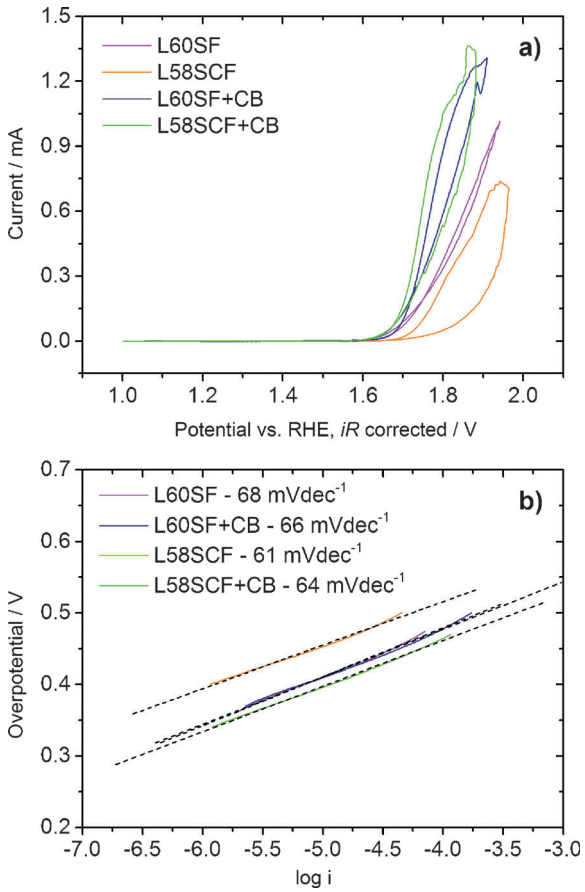

Figure 7. a) Comparison of CVs for L60SF and L58SCF, both without and with CB addition, in 0.1 M KOH. Scan rate: 5 mV s^{-1}. b) Tafel plots obtained from LSV recorded at 1 mV s^{-1}.

1.8 V vs. RHE). Moreover, a slight shift of approximately 60 mV was observed in the onset potential of OER in the case of L58SCF, which was due to the improved contact between the catalyst and the electrode. The slight changes in the Tafel slope are a good indication that the presence of CBs did not affect the kinetics or mechanism of the OER, and that the catalytic properties of the perovskites remained the same. The increase in current can be attributed to an enhancement in the availability of active sites due to the improved electrical contact by means of the conductive additive. Hence, the CBs only contributed to the results in terms of increasing conductivity and not enhancing the catalytic properties of the perovskites.

3. Conclusions

Fourteen perovskite samples were prepared and evaluated with respect to their catalytic activity for OER in alkaline media. Eight of these samples were catalytically active towards the electrochemical evolution of oxygen with overpotentials as low as 350 mV. Both the presence of specific cations (e.g. La and Co) and their stoichiometry played an essential role in the manifestation of OER activity. AFM imaging confirmed that the bubble formation led to catalyst detachment from the electrode surface. Enhancement of the current was achieved by inverting the conventional rotating disk electrode (RDE)-type electrode to allow for an easier bubble departure from the electrode surface, and therefore elude high blockage of the active catalyst layer. Further improvement of the electrode preparation and testing was carried out with selected catalysts (L60SF and L58SCF) by addition of a conductive material. The use of such additives provided additional contact sites between the catalyst particles and the glassy carbon supporting material, leading to an increase in the current (i.e. oxygen evolved) and reducing the overpotential required for OER in the case of L58SCF.

Experimental Section

Synthesis of Perovskite-Type Oxides

For the preparation of all perovskite powders nitrate salts were used as starting materials and dissolved in distilled water. From the individual solution of each cation, the corresponding stoichiometric amounts were combined to obtain a stock solution for each perovskite composition. After homogenization, the solution was spray-pyrolyzed in a commercial spray dryer (Nubilosa) with a throughput of 7.2 L h^{-1} corresponding to about 3 kg h^{-1} of the raw product. After spray pyrolysis the raw powder was calcined at $T = 900\,^{\circ}C$ in air for 5 h. After a short milling process to destroy the

spray granules, the powders were sintered at $T=1100\,^{\circ}C$ for 3 h to obtain crystallized materials.

Particle-Size Distribution, XRD, and BET Measurements

The powders were ball-milled for 6 h to obtain comparable particle size distributions. The particle size distribution was measured after ultrasonic treatment of the samples with a laser diffraction particle size analyzer Horiba LA950 V2 (Horiba).

A Bruker D4 Endeavor diffractometer with Cu K_α radiation was used for recording X-ray powder diffraction patterns of each perovskite powder in the 2θ-diffraction angle range from 10 to 80°. Phase analysis was performed with the PANalytical software "Highscore Plus", and refinements were performed by using the software packages "Jana" (Academy of Sciences, Institute of Physics, Prague, Czech Republic) or "GSAS".[23] Static N_2 physisorption measurements were carried out at $T=77$ K using an Autosorb-1 MP Quantachrome system to determine the BET specific surface area of all samples.

Preparation of Electrodes

For all electrochemical experiments a glassy carbon (GC) RDE-type electrode was used (4 mm diameter). Electrodes were polished to a mirror finish with a diamond slurry (3 μm) and alumina slurry (1 μm and 0.3 μm), before each measurement. All perovskite samples were ball milled (low power ball miller) for 10 min in order to separate particle aggregates and to obtain homogeneous powders for preparing catalyst inks. Electrochemical characterization was performed using thin-film type electrodes. Catalyst inks were prepared using Nafion as the binder (Nafion 117 ≈5% in alcohol mixture). The inks were prepared to a concentration of 5 mg mL^{-1} catalyst, with the solvent containing ultrapure water (49% volume ratio), ethanol (49% volume ratio), and Nafion (2% volume ratio). For preparing the catalyst layer, the ink of each sample (5 μL) was cast on the surface of the GC electrode and left to dry in air. Additional catalyst inks for selected perovskites were prepared in a similar fashion (same volume ratios) but with the addition of carbon black as a conductive additive (Vulcan® XC-72 Cabot Corporation, 237 m^2 g^{-1} BET surface area) to a final concentration of 1 mg mL^{-1}.

Electrochemical Characterization

All electrochemical measurements were performed in a three-electrode cell configuration using a PGSTAT30 or PGSTAT302N potentiostat/galvanostat (Metrohm Autolab).

The supporting electrolyte was 0.1 M NaOH or 0.1 M KOH. A Pt-wire served as the counter electrode and a commercial Ag/AgCl (3 M KCl) was used as the reference electrode. All potentials were converted to RHE according to [Eq. (1)]:

$$E_{RHE} = E_{Ag/AgCl} + 0.059pH + E^{\circ}_{Ag/AgCl} \quad (1)$$

Preliminary CV characterization was performed in a conventional setup in which the working electrode faced downwards. For the following experiments, from which Tafel slope parameters were extracted, an inverted working electrode configuration was used. In this way, the working electrode was facing upwards and the bubble departure from the surface of the electrode was facilitated. This configuration also minimized detachment of the catalyst films from the electrode due to gas evolution.

CVs were recorded between 0 and 1 V versus Ag/AgCl (≈1 and 2 V vs. RHE) with a scan rate of 5 mV s^{-1}, in O_2-saturated and O_2-depleted (Ar-saturated) atmospheres for the preliminary electrochemical characterization. All other experiments were performed in an Ar-saturated atmosphere. To saturate the solution with any of the gases, the electrolyte was bubbled for at least 15 min before the experiments, and a low stream of the gas was kept above the solution during measurement. Impedance spectroscopy was performed at open circuit potential (before CVs were performed) to determine the electrolyte resistance, and hence perform the *iR*-drop correction of the data. The spectra were recorded between 100 kHz and 500 mHz with a 10 mV amplitude of the ac perturbation. The electrolyte resistance was extrapolated from the high frequency impedance values. Tafel plots were constructed from the data obtained from slow linear sweep voltammetry (LSV). LSVs were recorded at 1 mV s^{-1} with a step potential of 0.1 mV in order to obtain steady-state current values. Overpotential values were calculated with respect to the thermodynamic potential of water oxidation (1.23 V vs. standard hydrogen electrode).

AFM Imaging

AFM was performed with a NanoWizard 3 equipped with a Vortis controller (JPK Instruments). The surface topography of the dried perovskite suspensions on GC was determined by tapping mode AFM in air with silicon cantilevers (NSC15, Mikromasch). Images were recorded before and after the electrochemical experiment, which included consecutive cycling (CVs) to observe changes in the catalyst layer after gas evolution. Electrodes identical to those used for electrochemical measurements were used as samples. The damping ratio was maintained at 80–90%, while both the sample and cantilever were grounded. For image analysis the software package belonging to the instrument was used (JPK Data Processing v. 4.2.53.).

Acknowledgements

The authors thank Dr. Y J. Sohn and M. Andreas (Forschungszentrum Jülich GmbH, IEK-1) for support in X-ray diffraction analysis and spray pyrolysis of ceramic powders; and Dr. Wei Xia (Laboratory of Industrial Chemistry, Ruhr Universität-Bochum) for support with BET measurements. Financial support by the Helmholtz Association through the "Initiative and Networking Fund" in the framework of the Helmholtz Energieallianz "Stationäre elektrochemische Feststoffspeicher und -wandler" (HA-E-0002) is gratefully acknowledged.

Keywords: alkaline media · electrocatalysis · electrochemical characterization · oxygen evolution reaction · perovskites

[1] R. F. Scarr, *J. Electrochem. Soc.* **1969**, *116*, 1526.
[2] S. Mitrovski, D. M. Drazic, *J. Serb. Chem. Soc.* **1998**, *63*, 555–564.
[3] G. Beni, L. M. Schiavone, J. L. Shay, W. C. Dautremont-Smith, B. S. Schneider, *Nature* **1979**, *282*, 281–283.
[4] T. Ioroi, N. Kitazawa, K. Yasuda, Y. Yamamoto, H. Takenaka, *J. Electrochem. Soc.* **2000**, *147*, 2018.
[5] L. da Silva, V. Alves, M. da Silva, S. Trasatti, J. Boodts, *Electrochim. Acta* **1997**, *42*, 271–281.
[6] A. Marshall, B. Børresen, G. Hagen, M. Tsypkin, R. Tunold, *Electrochim. Acta* **2006**, *51*, 3161–3167.
[7] S. Gottesfeld, S. Srinivasan, *J. Electroanal. Chem.* **1978**, *86*, 89–104.
[8] R. S. Yeo, *J. Electrochem. Soc.* **1981**, *128*, 1900.
[9] K. Izumiya, E. Akiyama, H. Habazaki, N. Kumagai, A. Kawashima, K. Hashimoto, *Electrochim. Acta* **1998**, *43*, 3303–3312.

[10] A. Tseung, S. Jasem, *Electrochim. Acta* **1977**, *22*, 31 – 34.
[11] Y. Matsumoto, E. Sato, *Electrochim. Acta* **1979**, *24*, 421 – 423.
[12] Y. Matsumoto, *J. Electrochem. Soc.* **1980**, *127*, 811.
[13] A. Kobussen, F. van Buren, T. van den Belt, H. van Wees, *J. Electroanal. Chem.* **1979**, *96*, 123 – 125.
[14] A. Mai, V. Haanappel, S. Uhlenbruck, F. Tietz, D. Stover, *Solid State Ionics* **2005**, *176*, 1341 – 1350.
[15] C. Jin, X. Cao, L. Zhang, C. Zhang, R. Yang, *J. Power Sources* **2013**, *241*, 225 – 230.
[16] J. O'M. Bockris„ T. Otagawa *J. Electrochem. Soc.* **1984**, *131*, 290 – 302.
[17] W. Zhou, J. Sunarso, *J. Phys. Chem. Lett.* **2013**, *4*, 2982 – 2988.
[18] a) A. Grimaud, K. J. May, C. E. Carlton, Y. L. Lee, M. Risch, W. T. Hong, J. Zhou, Y. Shao-Horn, *Nat. Commun.* **2013**, *117*, 25926 – 25932; b) J. I. Jung, H. Y. Jeong, J. S. Lee, M. G. Kim, J. Cho, *Angew. Chem.* **2014**, *18*, 4670 – 4674; *Angew. Chem. Int. Ed.* **2014**, *53*, 4582 – 4586.
[19] a) M. Komo, A. Hagiwara, S. Taminato, M. Hirayama, R. Kanno, *Electrochemistry* **2012**, *80*, 834 – 838; b) H. Ohkuma, I. Uechi, N. Imanishi, A. Hirano, Y. Takeda, O. Yamamoto, *J. Power Sources* **2013**, *223*, 319 – 324; c) W. G. Hardin, D. A. Slanac, X. Wang, S. Dai, K. P. Johnston, K. J. Stevenson, *J. Phys. Chem. Lett.* **2013**, *4*, 1254 – 1259; d) T. Takeguchi, T. Yamanaka, H. Takahashi, H. Watanabe, T. Kuroki, H. Nakanishi, Y. Y. Orisaka, Y. Uchimoto, H. Takano, N. Ohguri, M. Matsuda, T. Murota, K. Uosaki, W. Uead, *J. Am. Chem. Soc.* **2013**, *135*, 11125 – 11130; e) M. Risch, K. A. Soerzinger, S. Maruyama, W. T. Hong, I. Takeuchi, Y. Shao-Horn, *J. Am. Chem. Soc.* **2014**, *136*, 5229 – 5232.
[20] a) J. Suntivich, H. A. Gasteiger, N. Yabuuchi, H. Nakanishi, J. B. Goodenough, Y. Shao-Horn, *Nat. Chem.* **2011**, *3*, 546 – 550; b) J. Suntivich, K. J. May, H. A. Gasteiger, J. B. Goodenough, Y. Shao-Horn, *Science* **2011**, *334*, 1383 – 1385.
[21] a) J. M. Serra, V. B. Vert, M. Betz, V. A. C. Haanappel, W. A. Meulenberg, F. Tietz, *J. Electrochem. Soc.* **2008**, *155*, B207; b) F. Tietz, I. A. Raj, M. Zahid, A. Mai, D. Stöver, *Prog. Solid State Chem.* **2007**, *35*, 539 – 543.
[22] S. Trasatti, *Electrochim. Acta* **1984**, *29*, 1503 – 1512.
[23] I. C. Man, H.-Y. Su, F. Calle-Vallejo, H. A. Hansen, J. I. Martínez, N. G. Inoglu, J. Kitchin, T. F. Jaramillo, J. K. Nørskov, J. Rossmeisl, *ChemCatChem ChemCatChem.* **2011**, *3*, 1159 – 1165.
[24] a) V. A. C. Haanappel, A. Mai, S. Uhlenbruck, F. Tietz, *J. Fuel Cell Sci. Tech.* **2009**, *6*, 11007; b) V. A. C. Haanappel, B. Bär, C. Tropartz, J. Mertens, F. Tietz, *J. Fuel Cell Sci. Tech.* **2010**, *7*, 61017; c) *Proc., v. 2001 – 16*, (Eds.: S. C. Singhal, H. Yokokawa), Electrochem. Soc., Pennington, NJ, **2001**.
[25] V. A. C. Haanappel, N. Jordan, A. Mai, J. Mertens, J. M. Serra, F. Tietz, S. Uhlenbruck, I. C. Vinke, M. J. Smith, L. G. J. de Haart, *J. Fuel Cell Sci. Tech.* **2009**, *6*, 21302.
[26] A. C. Larson, R. B. Von Dreele, *Los Alamos National Laboratory Report LAUR* **2004**, 86 – 748.

Received: May 17, 2014
Published online on July 13, 2014